2015

Spectral diffusion map approach for structural health monitoring of wind turbine blades using distributed sensors

Venkatesh Chinde
Iowa State University

Spectral diffusion map approach for structural health monitoring of wind turbine blades using distributed sensors

by

Venkatesh Chinde

A thesis submitted to the graduate faculty

in partial fulfillment of the requirements for the degree of

MASTER OF SCIENCE

Major: Electrical Engineering

Program of Study Committee:

Umesh Vaidya, Major Professor

Simon Laflamme

Soumik Sarkar

Iowa State University

Ames, Iowa

2015

TABLE OF CONTENTS

LIST OF FIGURES

ABSTRACT

Distributed Sensor Networks (DSN) has emerged as a sensing paradigms in the structural egineering field due to the application of Structural Health Monitoring (SHM) for large-scale structures which results in accurately diagnosing the health of structures and enhancing the re liability and robustness of monitoring systems. The multisensor network greatly enhances the feasibility of applying SHM and also provides awareness of structural damage. In this work, we develop data-driven method for the diagnosis of damage in mechanical structures using an array of distributed sensors. The proposed approach relies on comparing intrinsic geometry of data sets corresponding to the undamage and damage state of the system. This approach assumes no knowledge of underlying models of the different data sources. We use spectral diffusion map approach for identifying the intrinsic geometry of the data set. In particular, time series data from distributed sensors is used for the construction of diffusion map. The low dimensional embedding of the data set corresponding to different damage level is done using singular value decomposition of the diffusion map to identify the intrinsic geometry. We construct appropriate metric in diffusion space to compare the low-dimensional data set corresponding to different damage cases. The developed algorithm is applied for damage diagnosis of wind turbine blades. Towards this goal we developed a detailed finite element-based model of CX-100 blade in ANSYS using shell elements. The damage in the blade is modeled by degrading the material property which in turn results in change of stiffness. One of the main challenges in the development of health monitoring algorithms is the ability to use sensor data with relatively small signal to noise ratio. Our developed diffusion map-based algorithm is shown to be robust to the presence of sensor noise. The proposed diffusion map-based algorithm can not only account for data from different sensors but also different types of sensor in the form of sensor fusion hereby making it attractive to exploit the distributed nature of sensor array. The distributed nature of sensor array is further exploited to determine the location of

damage on the wind turbine blade. Our extensive simulation results show that our proposed algorithms can not only determine the extend of damage but also the location of the damage.

CHAPTER 1. INTRODUCTION

Structural health monitoring (SHM) of large-scale systems, or mesosystems, including energy structures (e.g., wind turbine, dam), transportation infrastructures (e.g., bridge, pavement), and mechanical systems (e.g., aircraft, ship) is a difficult task due to the large geometries under inspection. Nevertheless, SHM at the mesoscale may have strong economic benefits. It has the potential to enable condition-based maintenance, instead of traditional time-based or breakdown-based strategies that are far less effective in terms of prolonging structural life. In particular, economic benefits for wind turbine blades are well understood Chang et al. (2003); Ciang et al. (2008); Adams et al. (2011).

To cope with the mesoscale challenge, off-the-shelf sensing strategies need to be adapted to provide large-area sensing capabilities Kharroub et al. (2015). A solution is to deploy distributed sensor networks (DSNs), which include wireless Swartz et al. (2010); Pakzad et al. (2008) and multivariate Wang et al. (2006); Torres-Arredondo et al. (2013); Malekzadeh et al. (2013); García et al. (2015) networks, as well as dense arrays of sensors Laflamme et al. (2013, 2012b); Ubertini et al. (2014); Glisic and Verma (2011); Ruan et al. (2014) that mimic biological skins, where changes in a local state can be monitored over a global area. The application of DSNs for SHM purposes typically leads to a significant quantity of data that needs to be processed strategically in order to obtain features related to structural condition. This is generally done using physics-driven or data-driven methods. While physics-driven methods typically lead to more accurate prognosis, they often rely on complex models that require long computation time. Conversely, data-driven methods can be operated in real-time and can be used to quickly detect a change in a condition, but yield results that may be difficulty to relate to structural behaviors Farrar and Lieven (2007).

The objective is to develop a condition assessment method for mesoscale systems that

leverages the utilization of DSNs and fuses sensor data into a condition index. We selected a data-driven method due to the fast computational time that may lead to real-time applications. The method is based on spectral diffusion maps. Diffusion maps belongs to unsupervised learning algorithms dealing with a spectral analysis of non-linear data and requires no prior knowledge regarding the appearance of damage, and no use is made of training data. With this method, the intrinsic geometries of the data sets obtained from DSNs are compared to identify potential changes in the system states, which would indicate damage. The intrinsic geometry of the data set is obtained using the multiscale diffusion map approach developed in Coifman et al. (2005). The diffusion-map method provides an embedding of the time-series data set in the diffusion space to identify important lower dimensional dynamic features of data. We construct appropriate metrics in the diffusion space to compare the embedded data under normal and abnormal operating conditions.

In the following we provide a brief overview of literature on comparison of intrinsic geometry of data sets. In Moniz et al. (2005), a multivariate attractor-based approach is used to detect the presence and magnitude of damage in structures through the investigation of the response's phase-space constructed by a time delayed embedding. A metric is introduced to quantify the damage-sensitive feature by comparing with the attractor of the undamaged structural response. Ref. Overbey et al. (2007) used the attractor constructed from the undamaged state to predict structural response, and identified damage as a change in the prediction error. An approach Monroig (2009) applied the theory to large nonlinear systems by dividing the system into a set of subsystems, and time series responses of each subsystem analyzed to identify damage. The authors in Figueiredo et al. (2010) proposed to analyze nonlinear time series using a multivariate autoregressive (MAR) approach in order to detect damage under varying operational and environmental conditions. Ref. Liu et al. (2013) used a combined state-space embedding strategy and singular value decomposition to detect structural damage. In Rabin and Averbuch (2010), a diffusion map-based approach was used for detection of anomaly in dynamic systems Rabin and Averbuch (2010). Ref. Huang et al. (2013) proposed a variation of diffusion maps termed discriminant diffusion maps analysis (DDMA) machine condition monitoring and fault diagnosis. The algorithm for diffusion map-based data comparison used

in this thesis was first presented in Vaidya et al. (2005). In Coifman and Hirn (2014), the theoretical basis for the construction and comparison of diffusion maps for family of data set changing with respect to change in system parameters is provided.

The diffusion map-based approach presented in this thesis combines ideas from variety of methods currently adopted for data-driven schemes for health monitoring such as spectral graph theory, Kernel methods, and machine learning. One of the important advantages of the proposed diffusion map-based approach is that it can be used for sensor data fusion. The presented algorithms exploit the distributed nature of sensor data in the form of sensor fusion. Comparison based on fused data from multiple sensors has the advantage that it is relatively robust to sensor noise thereby making it attractive in dealing with sensors with small signal-to-noise (SNR) ratio. Furthermore, DSN also provides an opportunity to localize the damage on the structure. Most of damage localization methods are applicable at a localized area, but not economically feasible in a large-scale structure Laflamme et al. (2012a). Damage localization in structures allows for considerable reduction of expenses related to their operation as well as increase in safety and longer lifespan. We show that our proposed approach successfully makes use of DSN to localize the damage on a wind turbine blade. The main contributions of this thesis are as follows. A nonlinear dimensionality-reduction framework using diffusion maps for structural condition assessment based on the intrinsic geometries of the data is proposed. This approach provides a low dimensional representation for a given set of heterogenous sensors which combines all the sensor information and the metric constructed is used to measure the connectivity in data points and achieves relatively robustly with respect to sensor noise. We also demonstrate that the proposed approach is well suited for identifying and locating the damage in the structures using DSN.

CHAPTER 2. DIFFUSION MAP

In this chapter, we provide the background on diffusion maps, which constitute the basis of our approach. The theory presented is a summary of work from Coifman et al. (2005); Lafon (2004).

2.1 Diffusion Map and algorithm

The construction of diffusion maps starts with the construction of a kernel function, $k(x, y)$, on set of data points Γ, where x and y are data points and belongs to space Γ. The kernel function $k(x, y)$ is constructed satisfying the following properties:

- k is symmetric, i.e., $k(x, y) = k(y, x)$
- k is positivity preserving i.e., $k(x, y) \geq 0$ for all x, y in Γ.
- k is positive semidefinite for all real valued bounded function f defined on the data set Γ,

$$\int_{\Gamma}\int_{\Gamma} k(x, y)f(x)f(y)d\mu(x)d\mu(y) \geq 0, \tag{2.1}$$

  where μ is a probability measure on Γ

The kernel function $k(x, y)$ is constructed based on local connectivity of data points and hence capture the local geometry of data set. Several choices for the kernel k are possible, all leading to different analyzes of data, we use the Gaussian or exponential form for the kernel function. The kernel function is used for the construction of the global geometry of data. The first step towards the construction of the diffusion map is to normalize the kernel function $k(x, y)$ as follows Chung (1997). For all $x \in \Gamma$

$$\text{let} \quad v^2(x) = \int_{\Gamma} k(x, y)d\mu(y),$$

and set

$$\tilde{a}(x,y) = \frac{k(x,y)}{v^2(x)}.$$

It follows from the construction that $\int_\Gamma \tilde{a}(x,y)d\mu(y) = 1$. To $\tilde{a}$ we can associate a linear operator on the data set Γ as follows:

$$\tilde{A}f(x) = \int \tilde{a}(x,y)f(y)d\mu(y). \tag{2.2}$$

Since we are interested in the spectral properties of the operator, it is preferable to work with a symmetric conjugate of $\tilde{A}$. We conjugate $\tilde{a}$ by v in order to obtain a symmetric form and we consider

$$a(x,y) = \frac{k(x,y)}{v(x)v(y)},$$

and the operator

$$Af(x) = \int_\Gamma a(x,y)f(y)d\mu(y). \tag{2.3}$$

The operator A is termed diffusion operator. Under very general hypotheses, the operator A is compact and self-adjoint. Thus, by spectral theory, we have

$$a(x,y) = \sum_{j\geq 0} \lambda_j \varphi_j(x)\varphi_j(y), \quad A\varphi_j(x) = \lambda_j\varphi_j(x). \tag{2.4}$$

where $\varphi_j(x)$ are eigenfunctions of A corresponding to eigenvalue λ_j. Let $a^m(x,y)$ be the kernel of A^m, then at the level of data points the kernel $a^m(x,y)$ has a probabilistic interpretation as a Markov chain with transition matrix a to reach y from x in m steps. Now define a mapping $\Phi : \Gamma \to \ell^2(N)$ as

$$\Phi(x) = (\varphi_0(x), \varphi_1(x), ..., \varphi_p(x), ...),$$

mapping the data point $x \in \Gamma$ into the Euclidean space $(\ell^2(N))$, which we will call the diffusion space. Each eigenfunction can be interpreted as a coordinate on the set. The diffusion distance in the original space Γ can now be defined using the mapping Φ. In particular, diffusion distance between two points $x, y \in \Gamma$ after m time steps is defined as follows

$$D_m^2(x,y) = \sum_{j\geq 0} \lambda_j^m(\varphi_j(x) - \varphi_j(y))^2. \tag{2.5}$$

Note that the diffusion distance between two points in the original space Γ is simply the Euclidean distance in the diffusion space. The diffusion distance measures the local connectivity

between the points in the underlying data set. Its value depends on the number of connecting paths between data points.

The diffusion map is used to map coordinates between data and the diffusion space, and can be exploited for dimensionality reduction. Dimensionality reduction can be conducted from the embedding generated by the eigenfunctions. For a given accuracy δ we retain only the eigenvalues $\lambda_0, ..., \lambda_{p-1}$ that, when raised to the power m, exceed a certain threshold (related to delta), and we use the corresponding eigenfunctions $\varphi_0, \varphi_1, ..., \varphi_{p-1}$ to embed the data points in R^p.

2.2 Comparison of data sets using Diffusion Map

The underlying idea behind the comparison of data sets using the diffusion map approach is adopted from Vaidya et al. (2005). For the simplicity of presentation, we will explain the comparison procedure between two data sets X and Y. The procedure for comparison involving multiple data sets is straight forward. Let $X = \{x_1, x_2, ..., x_N\}$ and $Y = \{y_1, y_2, ..., y_N\}$ be the two data sets obtained in the form of time series from an experiment or model simulation. We are assuming that the two data sets are of the same size, as this is our case of interest. However, the approach can be extended to the case when data sets are of different sizes Coifman and Hirn (2014). Using time-delayed coordinates, we embed the time series data in R^n, where n is sufficiently large. Now we have $N - n$ data points denoted by $\bar{X} := \{\bar{x}_1, \bar{x}_2, ..., \bar{x}_{N-n}\}$, $\bar{Y} := \{\bar{y}_1, \bar{y}_2, ..., \bar{y}_{N-n}\}$, where $\bar{x}_k = (x_k, x_{k+1}, ..., x_{k+n-1})$ and $\bar{y}_k = (y_k, y_{k+1}, .., y_{k+n-1})$. We denote the union of these two data sets by $Z = \{\bar{X}, \bar{Y}\}$. We use the following Gaussian kernel function,

$$k(z_k, z_j) = exp\left(-\frac{\parallel z_k - z_j \parallel^2}{\epsilon}\right), \tag{2.6}$$

The parameter ϵ is important in the computation of the Gaussian kernel. It is highly data dependent and specifies the size of the neighborhoods defining the local geometry of the data. The smaller the parameter ϵ, the faster the exponential decreases and hence the weight function in (2.6) becomes numerically insignificant as we move away from the center. It is easy to verify that the Gaussian kernel satisfies all the properties of the kernel.

From this kernel, we construct the diffusion operator or the diffusion matrix as follows. Assuming the transition probability between points z_k, z_j is proportional to $k(z_k, z_j)$, we can construct the Markov matrix as follows

$$M(k,j) = \frac{k(z_k, z_j)}{p(z_j)} \tag{2.7}$$

where $p(z_k)$ is the normalization constant given by

$$p(z_j) = \sum_k k(z_k, z_j) \tag{2.8}$$

Finally, the singular value decomposition is applied to M, yielding eigenvalues λ, which are sorted in descending order, and the corresponding eigenvectors φ. The eigenvalues of M lie in the range 0 to 1 due to normalization. Let $\{\varphi_1, \varphi_2, ..., \varphi_{2(N-n)}\}$ be the eigenvectors of the diffusion matrix and $\{\lambda_1, \lambda_2, ..., \lambda_{(N-n)}\}$ be the corresponding eigenvalues. Retaining only the first p eigenvectors and eigenvalues ($p = \max\{1 \in \mathbb{N} \text{ such that } |\lambda_l| > \delta|\lambda_1|\}, \delta > 0$ Coifman and Lafon (2006)) we can embed the data set Z in a p-dimensional Euclidean diffusion space, where $\{\varphi_1, ..., \varphi_p\}$ are the coordinates of the data points in the Euclidean space. Note that typically $p \ll n$ and hence we obtain the dimensionality reduction of the original data set. For some index j, the first $N-n$ elements of the eigenvector φ_j are the j-th coordinate in the diffusion space of the $N-n$ data points in X, while the remaining $N-n$ elements are the j-th coordinate in the diffusion space of the data set Y. Denote the eigenvector on data set X by φ^X and data set Y by φ^Y:

$$\varphi := \begin{bmatrix} \varphi^X \\ \varphi^Y \end{bmatrix}.$$

Note that the k-th elements of the j-th eigenvectors are given, respectively, by

$$\varphi^X_{kj} := \varphi^X_j(\bar{x}_k), \quad \varphi^Y_{kj} := \varphi^Y_j(\bar{y}_k). \tag{2.9}$$

We can use various metrics for the comparison of data sets in diffusion space using the above eigenvectors. We define

$$\phi^X_k = \left(\sum_{j=1}^{p} \lambda_j (\varphi^X_{kj})^2\right)^{\frac{1}{2}}, \ \phi^Y_k = \left(\sum_{j=1}^{p} \lambda_j (\varphi^Y_{kj})^2\right)^{\frac{1}{2}} \tag{2.10}$$

and propose following metric for the comparison of data sets.

1. *Weighted average diffusion distance*

$$D_{avg} = \left[\frac{1}{N-n}\sum_{k=1}^{N-n}\phi_k^X\right] - \left[\frac{1}{M-n}\sum_{k=1}^{M-n}\phi_k^Y\right] \tag{2.11}$$

2. *Pointwise diffusion distance*

$$D_p = \frac{1}{N}\sum_{k=1}^{N}\frac{\left|\phi_k^X - \phi_k^Y\right|}{\phi_k^X}. \tag{2.12}$$

This metric is sensitive to the ordering of the data set. Other metric can also be constructed depending upon application Moeckel and Murray (1997). For our proposed application of damage diagnosis of wind turbine blades, we employ the pointwise diffusion distance for data comparison in the diffusion space. This metric measures the diffusion distance between the data points in the original space and provides robust information on the geometry of the data set. The pointwise distance metric gives us satisfactory results. The proposed approach for the comparison of two data sets can be extended to multiple data sets in a straight forward manner Vaidya et al. (2005). For our proposed application, the different data sets will correspond to the different damage levels of a wind turbine blade. While the above procedure helps us compare different data sets corresponding to different damage levels, the procedure can be extended for comparison of data sets from multiple sensors. This can be accomplished using sensor fusion. We consider the case where the wind turbine blade is equipped with an array of distributed sensors. The goal is to fuse data from multiple sensors for damage diagnosis and also for damage localization.

2.3 Multiple sensor fusion

The procedure for sensor fusion in reconstructing the state of dynamical systems using diffusion maps is described in Keller et al. (2010). The strategy is to construct hierarchies of diffusion maps for a system consisting of heterogeneous sensors, where each sensor can be parameterized and normalized in its intrinsic diffusion coordinates, and a new graph is generated by combining all of the relevant diffusion coordinates from all the sensors. The algorithm for the multiple sensor fusion as it applies to our problem of damage detection is given below. The

algorithm closely follows one used in Rabin and Averbuch (2010) except for the comparison metric that is defined above in Eq. (2.12). For simplicity and conciseness, we will only consider the case of data fusion from three sensors.

2.3.1 Comparison of different damage data sets using multiple sensors

1. Let $X_i = \{x_1^i, x_2^i, ..., x_N^i\}$, $Y_i = \{y_1^i, y_2^i, ..., y_N^i\}$,and $Z_i = \{z_1^i, z_2^i, ..., z_N^i\}$ be the data sets from three sensors. The index $i = 0, 1, 2, 3...$ is the index for damage, with 0 is for undamaged case and N is the length of each data set. Using time delayed coordinates, we embed X_i for each i in $\mathbb{R}^n$ where n is sufficiently large.

2. We have $N - n$ data points for individual time series $\bar{X}_i := \{\bar{x}_1^i, \bar{x}_2^i, ..., \bar{x}_N^i\}$ where $\bar{x}_k^i = (x_k^i, x_{k+1}^i, ..., x_{k+n-1}^i)$ We denote the union of these data sets $\bar{X}_0, \bar{X}_1, ...$ as $\hat{X} = \{\bar{X}_0, \bar{X}_1, ...\}$

3. We apply the procedure outlined above to other sensors Y, Z, and we get $\hat{Y}$ and $\hat{Z}$

4. We apply the diffusion map to data set $\hat{X}$. The embedding coordinates of $\hat{X}$ are scaled and are denoted by Ψ_1 as $\Psi_1(x) = (\frac{\lambda_1\psi_1(x)}{\|\lambda_1\psi_1(x)\|}, \frac{\lambda_2\psi_2(x)}{\|\lambda_2\psi_2(x)\|}, \frac{\lambda_3\psi_3(x)}{\|\lambda_3\psi_3(x)\|}, ...)$

5. We repeat the above procedure for all of the different data sets $\hat{Y}$ and $\hat{Z}$, and the scaled embedding coordinates for $\hat{Y}$ and $\hat{Z}$ is given by Ψ_2 and Ψ_3.

6. The scaled diffusion coordinates are combined into a matrix form given by $W = \{\Psi_1, \Psi_2, \Psi_3\}$. The diffusion map is applied again on this matrix W.

7. We retain only the first p eigenvectors ($p \ll n$) of the diffusion matrix and $\{\lambda_1, \lambda_1, ..., \lambda_p\}$ corresponding eigenvalues, so that we can embed the data set W in a p-dimensional Euclidean diffusion space.

8. The resulting eigenvectors can be decomposed in the form of damage indices as $\hat{\varphi} = [\hat{\varphi}^0; \hat{\varphi}^1; \hat{\varphi}^2; ....]$

9. The pointwise diffusion distance is applied on these sets of eigenvectors in order to capture the varying degrees of damage in the system.

A schematic of the sensor fusion approach is shown in Figure 2.1 using n sensors.

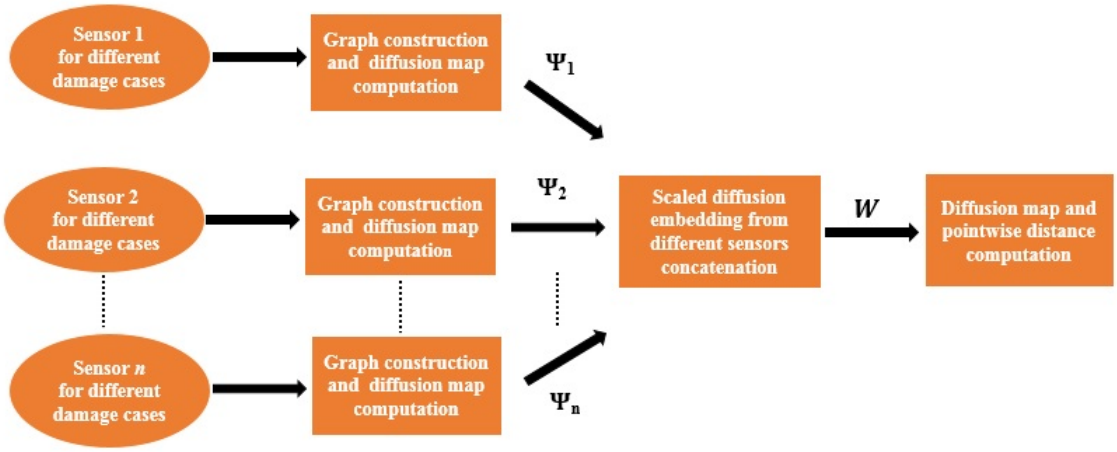

Figure 2.1 Sensor fusion using n sensors

CHAPTER 3. WIND TURBINE BLADE MODELING

In this chapter, we present the numerical model used for the numerical analysis of the proposed method.

3.1 ANSYS model

The model consists of a wind turbine blade equipped with a DSN and subjected to various wind loads, described in what follows.

The wind turbine blade is modeled after the 9 m CX-100 carbon fiber blade described in Berry and Ashwill (2007). This particular blade has been widely studied White et al. (2010); Dervilis et al. (2014); Berry and Berg (2008). A simplified finite element model was generated in ANSYS using shell elements. It consists of a tapered cantilever plate of 9 m length, 1.03 m largest width, and 0.035 m thickness, as shown in Fig. 3.1. The blade is a composite assembled from 3 different layers constituted with 2 different materials and 3 different orientations, as listed in Table 3.1.

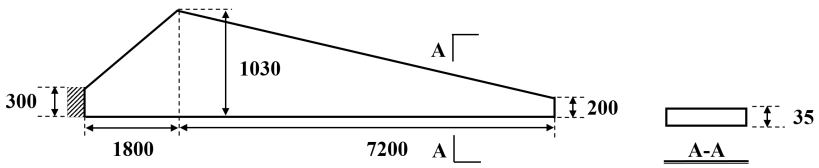

Figure 3.1 Wind turbine blade dimensions (mm) (a) top view; and (b) cross section.

Table 3.1 Material properties

Layer	Material (orientation)	E_x (GPa)	E_y (GPa)	G_{xy} (GPa)	density (kg/m^3)	thickness (mm)
1	Carbon-fiberglass fabric (+45°)	84.10	8.76	4.38	3469	13
2	C520 fiberglass (0°)	37.30	7.60	6.89	1874	9
3	Carbon-fiberglass fabric (−45°)	84.10	8.76	4.38	3469	13

The blade was modeled to match the first flatwise and edgewise frequencies of the experimental values reported in Ref. Berry and Berg (2008). The model and experimental values are compared in Table 3.2. The first frequencies of the model agree with the experimental values.

Table 3.2 Comparison of frequencies

direction	model (Hz)	experimental (Hz) Berry and Berg (2008)	difference (%)
flapwise	4.16	4.56	−8.8
edgewise	8.02	7.49	+7.1

3.2 Damage cases

Five different damage locations and severities are considered in the simulations. They are schematized in Fig. 3.2, in which the red-dashed regions represent the damaged element. Damage locations 1 to 4 (Fig. 3.2(a)-(d)) vary from the root (Fig. 3.2(a)) to the free end (Fig. 3.2(d)) of the blade, while damage location 5 (Fig. 3.2(e))) is a combination of damage locations 1 and 3. The blue dots represent the location of 9 virtual strain gauges constituting the DSN. They are equally spaced at 1 m and located in the middle of blade. Fig. 3.2(f) shows the cartesian coordinates of the nine virtual strain gauges.

The simulated damage is a loss of stiffness arising from delamination, a damage mode commonly studied in wind turbine blade literature Adams et al. (2011). It is modeled as a change in the stiffness of laminate layer 2. Five different damage severities are considered under damage location 1 (Fig. 3.2(a)), which correspond to changes in the first natural frequencies of 1%, 2%, 5%, 10% and 15% (35.5%, 54.8%, 80.6%, 92.3% and 96.7% stiffness loss in damaged elements in the strong bending direction). The damage localization study compares all locations

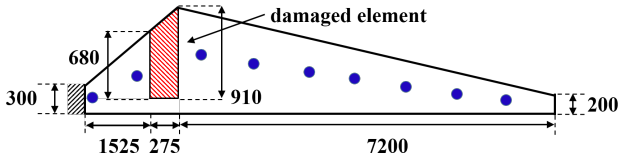

(a)

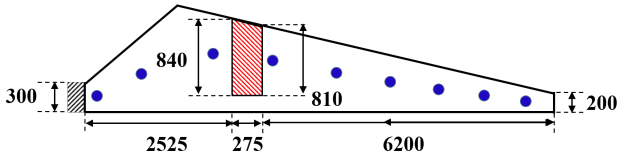

(b)

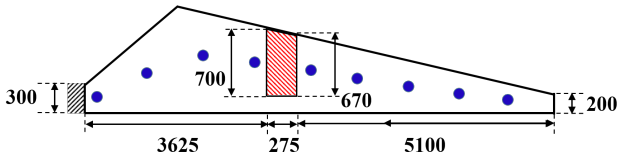

(c)

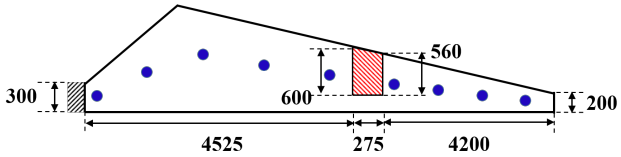

(d)

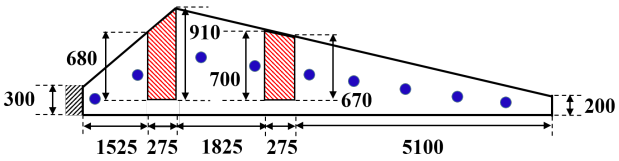

(e)

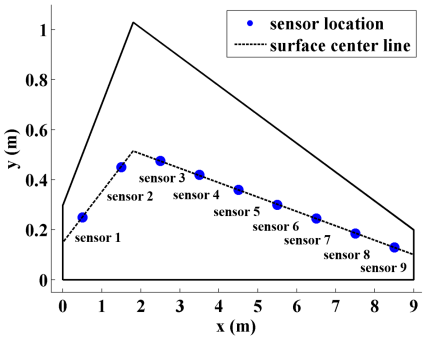

(f)

Figure 3.2 Damage locations under study: (a) location 1; (b) location 2; (c) location 3; (d) location 4; (e) location 5; and (f) sensors location.

under constant damage corresponding to a 10% change in the first natural frequency.

3.3 Wind Load model

The natural variability of the wind loading on the blade is generated using the procedure described in Ackermann et al. (2005). The wind speed W_s applied to the wind turbine blade is constituted from four components:

$$W_s = W_a + W_r + W_g + W_t, \tag{3.1}$$

where W_a is the average speed, W_r is the ramp component, W_g is the gust component, and W_t is the turbulence. The ramp component W_r is taken as

$$W_r = \begin{cases} 0 & \text{if} \quad t < T_{sr} \\ w_{\text{ramp}} & \text{if} \quad T_{sr} < t < T_{er} \\ 0 & \text{if} \quad t > T_{er}, \end{cases} \tag{3.2}$$

where $w_{\text{ramp}} = A_{\text{ramp}} \frac{(t-T_{sr})}{(T_{er}-T_{sr})}$ with A_{ramp} being the amplitude of wind speed ramp, T_{sr} and T_{er} are the starting and end time of wind speed ramp, respectively. The wind gust W_g is taken as

$$W_g = \begin{cases} 0 & \text{if} \quad t < T_{sg} \\ w_{\text{gust}} & \text{if} \quad T_{sg} < t < T_{eg} \\ 0 & \text{if} \quad t > T_{eg}, \end{cases} \tag{3.3}$$

where, $w_{\text{gust}} = A_{\text{gust}} \left(1 - \cos\left(2\pi \left(\frac{t-T_{sg}}{T_{eg}-T_{sg}}\right)\right)\right)$ with A_{gust} being the amplitude of wind gust, T_{sg} and T_{eg} are the starting and end time of wind gust, respectively. W_t is modeled as a one-dimensional random process and is characterized by the following power spectral density function $P(f)$ for a given frequency f Ackermann et al. (2005)

$$P(f) = l \cdot W_a \left(\ln\left(\frac{h}{z_0}\right)^2\right)^{-1} \left(1 + 1.5\frac{f \cdot l}{W_a}\right)^{-5/3},$$

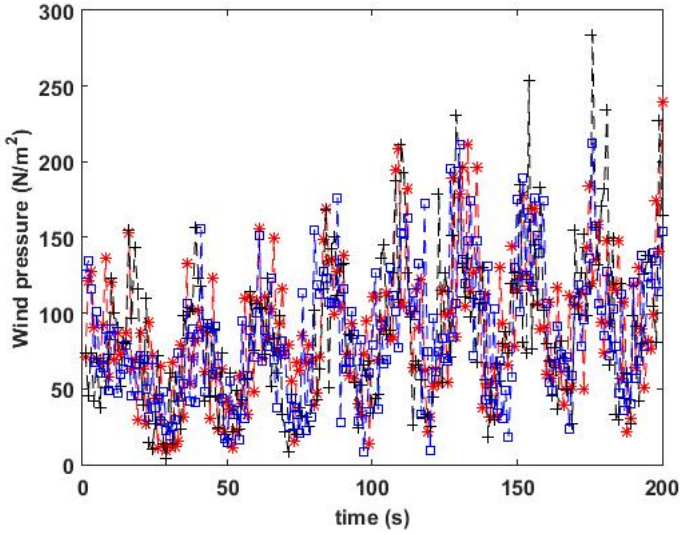

Figure 3.3 Three different realizations of wind pressure.

where l is the turbulence length scale, h is the height at which the wind speed is applied, and z_0 is the roughness length. The wind pressure acting on the blade is directly obtained from W_s using Van der Woude and Narasimhan (2010)

$$W_p = 0.5\rho W_s^2, \tag{3.4}$$

where ρ is the air density. The variability in wind speed at different heights across the blade is taken into account using the power law Peterson and Hennessey Jr (1978). The resulting wind pressure obtained (3.4) is applied onto the top surface of the wind turbine blade model. Table 3.3 lists the values of the selected parameters for the generation of different wind load realization. In order to take into account the uncertainty in wind speed, each damage case is simulated under three different wind pressure realization using the parameters listed in Table 3.3. A total of 30 different realizations are considered for the analysis. Fig. 3.3 shows three different realizations of wind pressure.

Table 3.3 Model parameters for wind load generation.

Parameter	Value
$T_{sr} = T_{sg}$	50 s
T_{er}	150 s
T_{eg}	200 s
h	70 m
A_{ramp}	4 m/s
A_{gust}	-3 m/s
l	600 m
z	0.01m
W_a	11.5 m/s

CHAPTER 4. SIMULATION RESULTS

In this chapter, we study the performance of the diffusion map algorithm at detecting different damage levels and locations.

4.1 Different damage levels

Figure 4.1 shows the study of the eigenvalues of the diffusion map obtain from sensor 1 only, for the undamaged blade subjected to a wind load realization. Other than the first eigenvalue at one, there are three dominating eigenvalues (choosing $\delta = 0.01$, we have $p = 3$, refer to paragraph below equation 8). Thus, the data set can be approximated using the three dominant eigenvectors of the diffusion map. The eigenvector plot corresponding to first three dominant eigenvalues for all the damage cases is shown in Fig. 4.1(b).

The exercise is repeated for sensor 2, which is the closest to the damage. Similarly to sensor 1, the study of the eigenvalues (Fig. 4.2(a)) shows three dominant eigenvalues. A plot of the eigenvectors of sensor 2 data set is shown in Fig. 4.2(b). A comparison between the eigenvector plots for sensor 1 (Fig. 4.1(b)) and sensor 2 (Fig. 4.2(b)) shows a more apparent change in the magnitude of the eigenvectors as the damage increases. This is largely attributed to the larger change in strain readings from sensor 2, as it is closer to the damage.

Figure 4.3 is a plot of the pointwise diffusion distances D_p for all the nine sensors as a function of different damage cases, where 0% corresponds to the undamaged case. As noted previously, three different wind load realizations were simulated for each damage case. The average data from three different wind realizations for each damage case is used for calculating the pointwise diffusion distance using the proposed approach. The results for each sensor shows an increasing D_p for an increasing damage level. The pointwise diffusion distance D_p

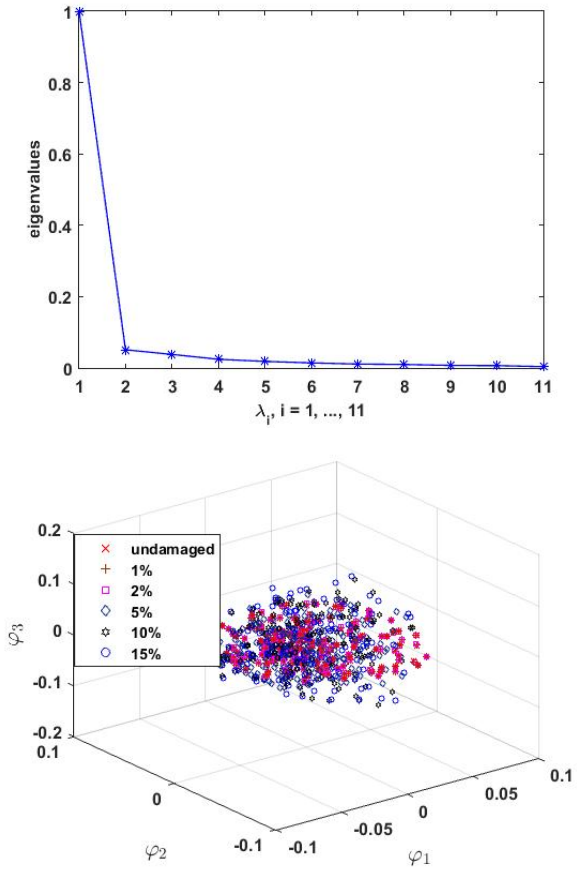

Figure 4.1 Sensor 1: (a) eigenvalues; (b) three dimensional embedding.

can therefore be utilized to detect and evaluate the gravity of damage. Sensor 2 (sen 2) exhibits a notably higher magnitude of D_p compared with other sensors. This demonstrates that D_p can also be utilized to localize damage.

The sensor fusion strategy described in chapter 2 can be used to provide a direct measure of damage. In Fig. 4.4, the information from all the 9 sensors is fused. Results show an increasing pointwise diffusion distance with increasing damage level. A relationship between D_{SF} and damage levels could be established to create a useful damage index, enabling damage prognosis.

Results discussed above demonstrate that the embedding of the map can be used for damage detection. This is also true for a simple comparison of strain readings. For instance, take an output-only strain comparison algorithm that consists of comparing the relative response

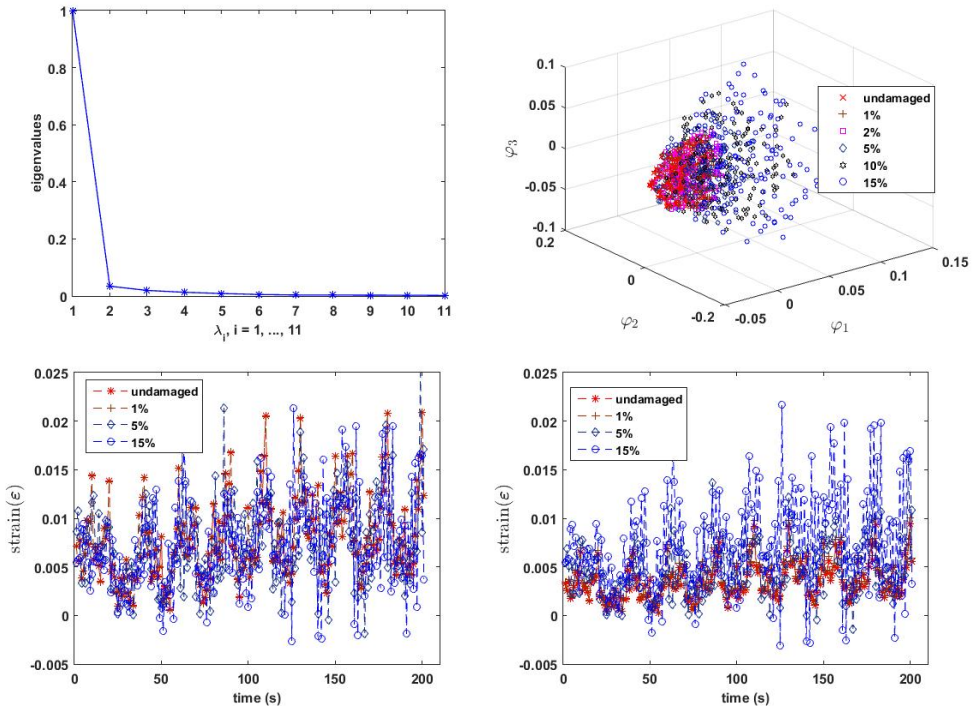

Figure 4.2 (a) eigenvalues; (b) three dimensional embedding; (c) strain measured by sensor 1; (d) strain measured by sensor 2.

between two sensors through events. Assuming that the response of the dynamic system is largely dominated by the first mode (not to confuse with dominating eigenvalues of the diffusion map), the relative strain $\varepsilon_i/\varepsilon_j$ between two points i and j remains approximately constant. Thus, we can write a performance index J:

$$J = \left| \left(\sum_{k=1}^{K} \frac{s_{i,k}}{s_{j,k}} - \sum_{k=1}^{K^*} \frac{s^*_{i,k}}{s^*_{j,k}} \right) \left(\sum_{k=1}^{K^*} \frac{s^*_{i,k}}{s^*_{j,k}} \right)^{-1} \right| \tag{4.1}$$

where $s_{i,k}$ is the signal of the sensor i at time k, which is compared with $s_{j,k}$, the signal of sensor j at time k, over the time series K. The star represents data associated with the undamaged case. This performance index J represents the change in the relative response between two sensors. Note that $s_{j,k}$ might not be limited to one sensor in the case where the comparison is conducted between two neighbors. The study on damage cases is repeated using this algorithm, where sensor i is compared with neighbors $i \pm 1$ for $i = 2, 3, ..., 8$ and $i + 1$ for $i = 1$ and $i - 1$ for $i = 9$. Figure 4.5 plots the value of J per sensor for different damage cases. Results show

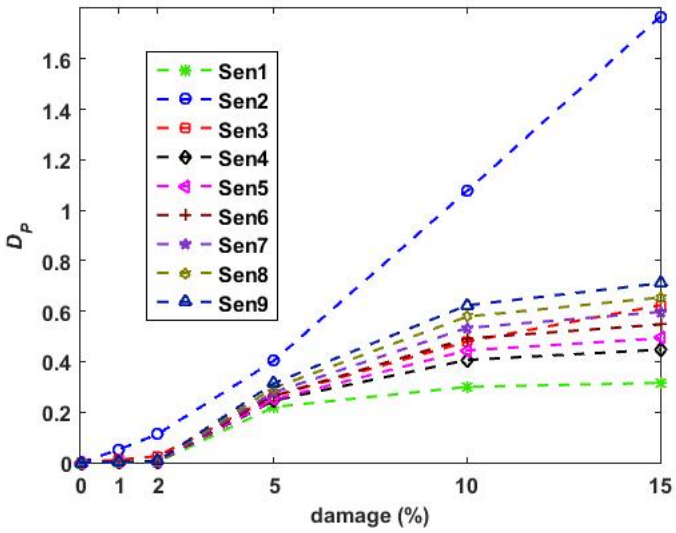

Figure 4.3 Pointwise distance for all sensors.

that damage is between sensors 1 and 2 or sensors 2 and 3 (highest J values). Also, similarly to the diffusion map algorithm, the J index can be used to detect, localize, and evaluate the gravity of damage. The comparison of the diffusion map algorithm with this simple study of the relative response will be useful, later in this section, to demonstrate the superior robustness of the proposed method.

4.2 Different damage locations

To further demonstrate the capacity of the diffusion map algorithm at localizing damage, the algorithm is simulated for the other damage locations discussed in section 3.2. Figure 4.6 is a plot of the pointwise diffusion distance values obtained by comparing against the undamaged cases, as a function of each sensor. The magnitude of D_p corresponding to sensor 2 is larger compared to all the sensors for location 1, sensor 3 for location 2, sensor 4 for location 3, sensor 5 for location 4, and sensors 2 and 4 for location 5. These values correspond to the closest sensors for each damage case, showing that the proposed methodology performs well at localizing each damage. The drift of that occurs at the end of the blade for each damage location is attributed to differences in the strain magnitudes with respect to the undamaged case.

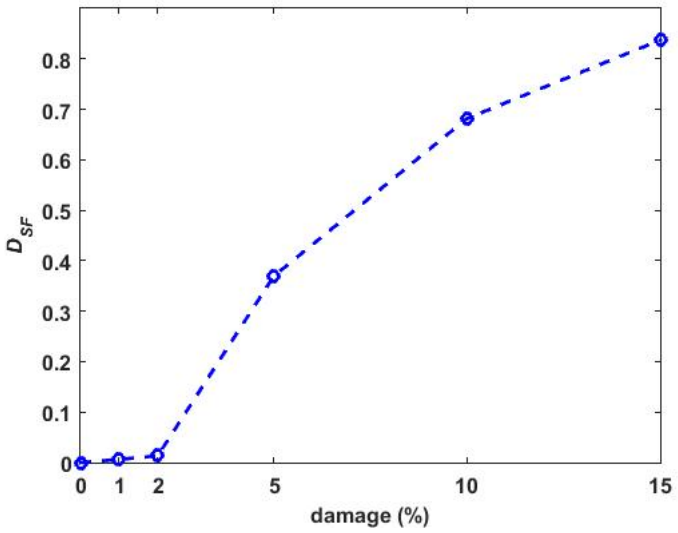

Figure 4.4 Pointwise distance using sensor fusion.

4.3 Robustness

The robustness of the diffusion map algorithm with respect to noise is investigated. Data sets are generated with different levels of noise: 0.1%, 1%, 5%, and 10%. The noisy data $s_{\text{noise}}(t)$ is generated from the actual data set $s_{\text{actual}}(t)$:

$$s_{\text{noise}}(t) = s_{\text{actual}}(t) + \sigma_{\text{noise}}\xi(t) \tag{4.2}$$

where the noise variance is given by $\sigma^2_{\text{noise}} = \frac{\sigma^2_{\text{signal}}}{\text{SNR}}$ and $\xi(t)$ is a normally distributed random variable. The value of SNR is varies to add different levels of noise to the actual data set. Figure 4.7 shows the diffusion distances at different damage levels under these levels of noise. At 0.1% and 1% noise levels, it is clear that sensor 2 has the largest value for D_p, enabling damage localization. However, beyond 5% noise, damage below 1% is difficult to localize. At 10% noise, damages under 1% are difficult to localize. Nevertheless, damages cases at and beyond 5% changes in the dominating frequency are clearly identified, even at a 10% noise level.

The study can be extended to the relative strain comparison algorithm discussed above. Figure 4.8 shows the evolution of performance index J as noise is increased. It becomes rapidly difficult to detect and localize data using this technique, which further exhibits the advantageous

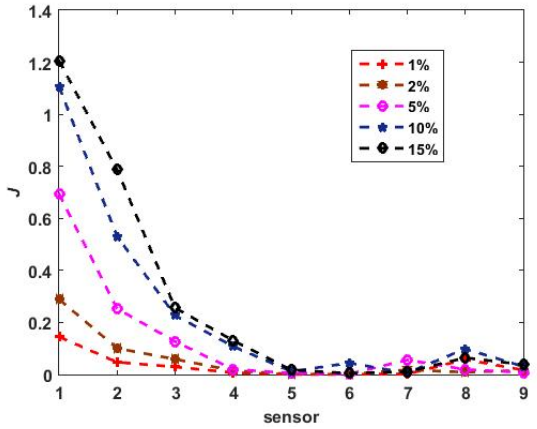

Figure 4.5 Performance J for various sensors.

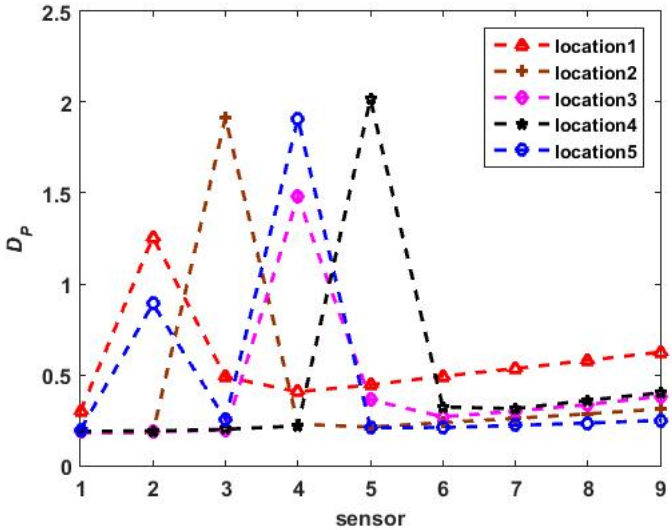

Figure 4.6 Pointwise distance for all sensors for damage localization.

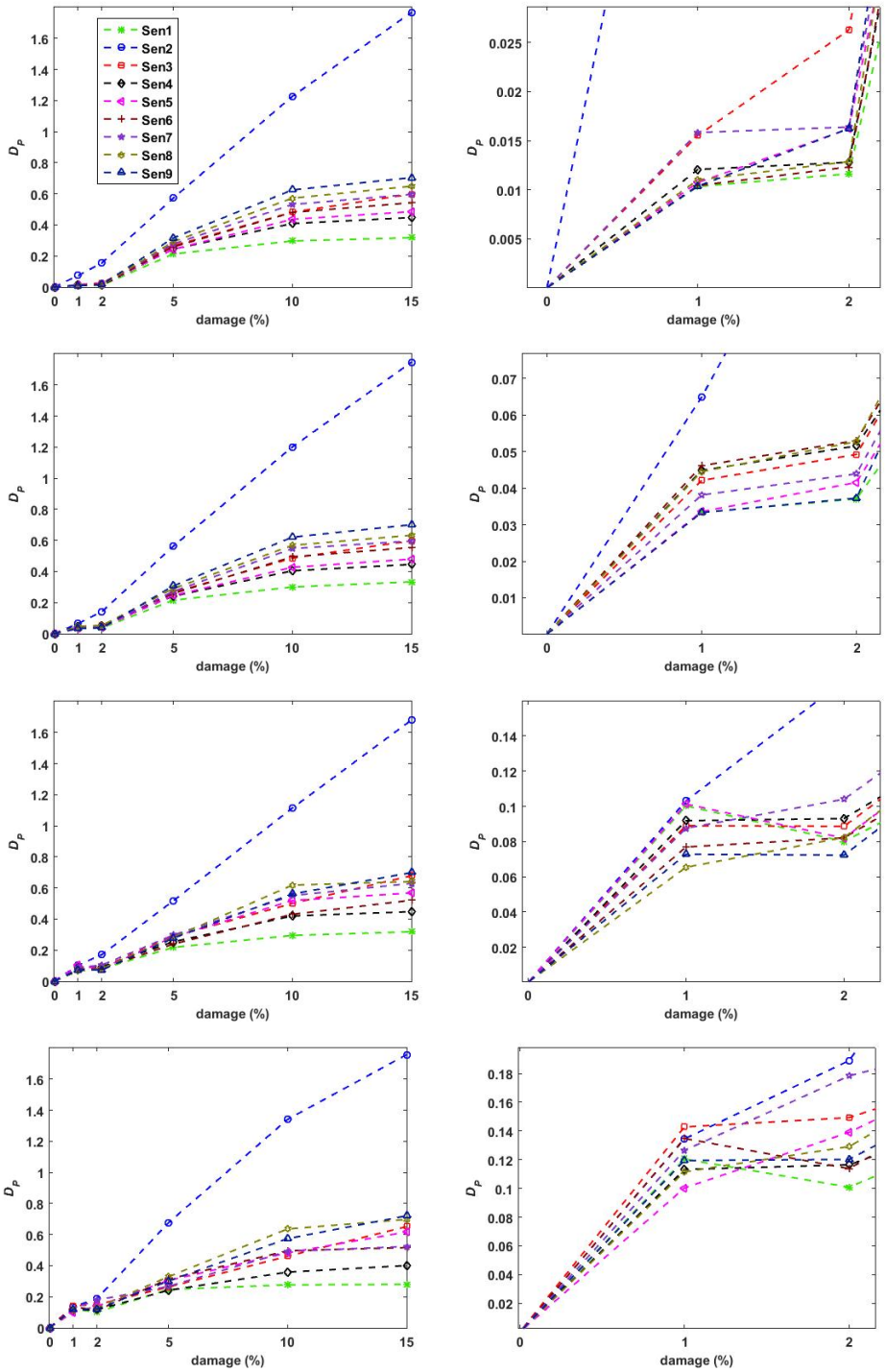

Figure 4.7 Pointwise distance for different noise levels $(0.1\%, 1\%, 5\%, 10\%)$.

robustness of the proposed method.

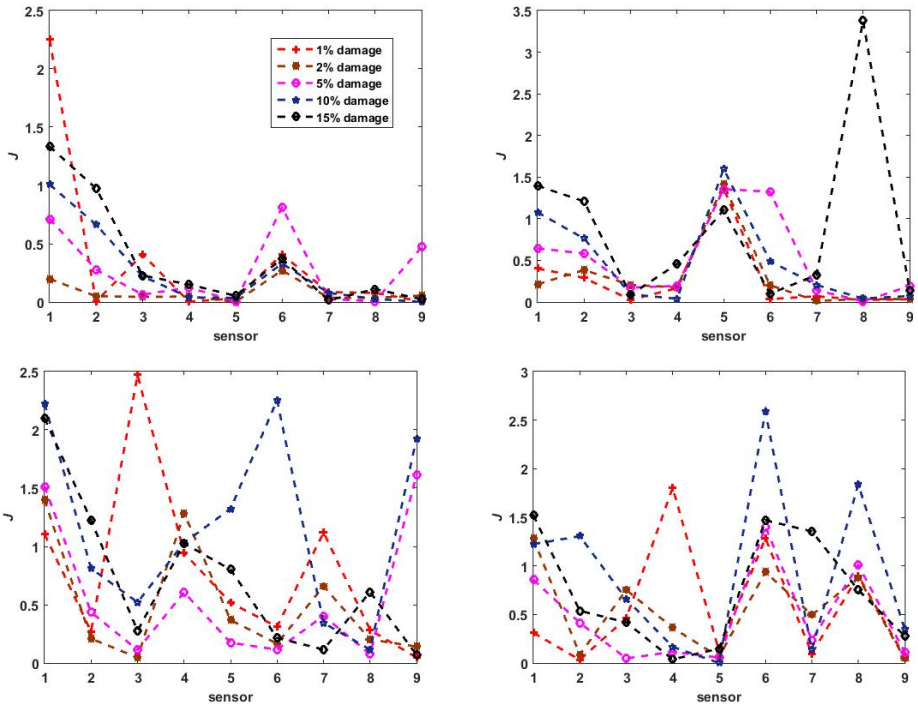

Figure 4.8 Performance J: (a) 0.1% percent; (b) 1% percent (c) 5% percent (d) 10% percent.

CHAPTER 5. CONCLUSION

In this work, we proposed a new approach enabling damage detection and localization on mesosystems. The approach consists of utilizing a sensor network combined with a spectral diffusion map-based method. With the diffusion maps, the intrinsic geometries between two data sets are compared, and a change in these geometries is an indicator of damage. The magnitude of such change can be used to compare the magnitude of damage, the first step towards prognosis. By comparing the diffusion distances at each sensor, it is also possible to localize damage. An algorithm for data fusion as been presented, which enables the combination of multiple data sets from a number of sensors, which may measure different states, for damage diagnosis.

The proposed method has been investigated via numerical simulations. These simulations were conducted on a realistic blade model subjected to different wind realizations. Different damage cases and localizations have been used to study the performance of the algorithm. Results showed that, without noise, the method was able to locate and detect damage as low as 0.1%. In the presence of noise, the method was able to locate and detect a 0.1% damage under a 1% noise level, and a 5% damage under a 10% noise level. Results were also compared with a simple comparison of relative responses between sensors, which failed at providing an acceptable damage detection and localization performance under noise. The data fusion algorithm was successful at providing an overall measure of damage.

This study demonstrated critical advantages of the proposed approach. First, the spectral diffusion map-based method can be combined with DSNs to locate and detect damage. Second, it can be used to fuse information from multiple sensors to provide a numerical value linked to a measure of damage gravity. Third, it is robust with respect to noise. It follow that the proposed approach has great potential for structural health monitoring of mesosystems.

BIBLIOGRAPHY

Ackermann, T. et al. (2005). *Wind power in power systems*, volume 140. Wiley Online Library.

Adams, D., White, J., Rumsey, M., and Farrar, C. (2011). Structural health monitoring of wind turbines: method and application to a hawt. *Wind Energy*, 14(4):603–623.

Berry, D. and Ashwill, T. (2007). Design of 9-meter carbon-fiberglass prototype blades: Cx-100 and tx-100. *SAND2007-0201, Sandia National Laboratories, Albuquerque, NM*.

Berry, D. S. and Berg, D. (2008). Blade system design studies phase ii: final project report. *Sandia Report SAND2008-4648*.

Chang, P. C., Flatau, A., and Liu, S. (2003). Review paper: health monitoring of civil infrastructure. *Structural health monitoring*, 2(3):257–267.

Chung, F. R. (1997). *Spectral graph theory*, volume 92. American Mathematical Soc.

Ciang, C. C., Lee, J.-R., and Bang, H.-J. (2008). Structural health monitoring for a wind turbine system: a review of damage detection methods. *Measurement Science and Technology*, 19(12):1–20.

Coifman, R. R. and Hirn, M. J. (2014). Diffusion maps for changing data. *Applied and Computational Harmonic Analysis*, 36(1):79–107.

Coifman, R. R. and Lafon, S. (2006). Diffusion maps. *Applied and computational harmonic analysis*, 21(1):5–30.

Coifman, R. R., Lafon, S., Lee, A. B., Maggioni, M., Nadler, B., Warner, F., and Zucker, S. W. (2005). Geometric diffusions as a tool for harmonic analysis and structure definition of data:

Diffusion maps. *Proceedings of the National Academy of Sciences of the United States of America*, 102(21):7426–7431.

Dervilis, N., Choi, M., Taylor, S., Barthorpe, R., Park, G., Farrar, C., and Worden, K. (2014). On damage diagnosis for a wind turbine blade using pattern recognition. *Journal of sound and vibration*, 333(6):1833–1850.

Farrar, C. and Lieven, N. (2007). Damage prognosis: the future of structural health monitoring. *Philosophical Transactions of the Royal Society A: Mathematical, Physical and Engineering Sciences*, 365(1851):623–632.

Figueiredo, E., Todd, M., Farrar, C., and Flynn, E. (2010). Autoregressive modeling with state-space embedding vectors for damage detection under operational variability. *International Journal of Engineering Science*, 48(10):822–834.

García, D., Tcherniak, D., and Trendafilova, I. (2015). Damage assessment for wind turbine blades based on a multivariate statistical approach. In *Journal of Physics: Conference Series*, volume 628, page 012086. IOP Publishing.

Glisic, B. and Verma, N. (2011). Very dense arrays of sensors for shm based on large area electronics. *Structural Health Monitoring*, pages 1409–1416.

Huang, Y., Zha, X. F., Lee, J., and Liu, C. (2013). Discriminant diffusion maps analysis: A robust manifold learner for dimensionality reduction and its applications in machine condition monitoring and fault diagnosis. *Mechanical Systems and Signal Processing*, 34(1):277–297.

Keller, Y., Coifman, R. R., Lafon, S., and Zucker, S. W. (2010). Audio-visual group recognition using diffusion maps. *Signal Processing, IEEE Transactions on*, 58(1):403–413.

Kharroub, S., Laflamme, S., Song, C., Qiao, D., Phares, B., and Li, J. (2015). Smart sensing skin for detection and localization of fatigue cracks. *Smart Materials and Structures*, 24(6):065004.

Laflamme, S., Kollosche, M., Connor, J., and Kofod, G. (2012a). Soft capacitive sensor for structural health monitoring of large-scale systems. *Structural Control and Health Monitoring*, 19(1):70–81.

Laflamme, S., Kollosche, M., Connor, J. J., and Kofod, G. (2012b). Robust flexible capacitive surface sensor for structural health monitoring applications. *Journal of Engineering Mechanics*, 139(7):879–885.

Laflamme, S., Saleem, H. S., Vasan, B. K., Geiger, R. L., Chen, D., Kessler, M. R., and Rajan, K. (2013). Soft elastomeric capacitor network for strain sensing over large surfaces. *Mechatronics, IEEE/ASME Transactions on*, 18(6):1647–1654.

Lafon, S. S. (2004). *Diffusion maps and geometric harmonics*. PhD thesis, Yale University.

Liu, G., Mao, Z., Todd, M. D., and Huang, Z. (2013). Damage assessment with state-space embedding strategy and singular value decomposition under stochastic excitation. *Structural Health Monitoring*, pages 131–142.

Malekzadeh, M., Gul, M., and Catbas, F. N. (2013). Application of multivariate statistically based algorithms for civil structures anomaly detection. In *Topics in Dynamics of Civil Structures, Volume 4*, pages 289–298. Springer.

Moeckel, R. and Murray, B. (1997). Measuring the distance between time series. *Physica D: Nonlinear Phenomena*, 102(3):187–194.

Moniz, L., Nichols, J., Nichols, C., Seaver, M., Trickey, S., Todd, M., Pecora, L., and Virgin, L. (2005). A multivariate, attractor-based approach to structural health monitoring. *Journal of Sound and Vibration*, 283(1-2):295–310.

Monroig, E. (2009). *Detection of Changes in Dynamical Systems by Nonlinear Time Series Analysis*. PhD thesis, University of Tokyo.

Overbey, L., Olson, C., and Todd, M. (2007). A parametric investigation of state-space-based prediction error methods with stochastic excitation for structural health monitoring. *Smart Materials and Structures*, 16:1621–1638.

Pakzad, S. N., Fenves, G. L., Kim, S., and Culler, D. E. (2008). Design and implementation of scalable wireless sensor network for structural monitoring. *Journal of Infrastructure Systems*.

Peterson, E. W. and Hennessey Jr, J. P. (1978). On the use of power laws for estimates of wind power potential. *Journal of Applied Meteorology*, 17(3):390–394.

Rabin, N. and Averbuch, A. (2010). Detection of anomaly trends in dynamically evolving systems. In *AAAI Fall Symposium: Manifold Learning and Its Applications*.

Ruan, J., Ho, S. C. M., Patil, D., Li, M., and Song, G. (2014). Wind turbine blade damage detection using an active sensing approach. *Smart Materials and Structures*, 23(10):105005.

Swartz, R. A., Lynch, J. P., Zerbst, S., Sweetman, B., and Rolfes, R. (2010). Structural monitoring of wind turbines using wireless sensor networks. *Smart structures and systems*, 6:0.

Torres-Arredondo, M. A., Tibaduiza-Burgos, D. A., Mujica, L. E., Rodellar, J., and Fritzen, C.-P. (2013). Data-driven multivariate algorithms for damage detection and identification: evaluation and comparison. *Structural Health Monitoring*, page 1475921713498530.

Ubertini, F., Laflamme, S., Ceylan, H., Materazzi, A. L., Cerni, G., Saleem, H., D'Alessandro, A., and Corradini, A. (2014). Novel nanocomposite technologies for dynamic monitoring of structures: a comparison between cement-based embeddable and soft elastomeric surface sensors. *Smart Materials and Structures*, 23(4):1–12.

Vaidya, U., Hagen, G., Banaszuk, A., Lafon, S., Mezic, I., and Coifman, R. R. (2005). Comparison of systems using diffusion maps. In *Proceedings of the 44th IEEE Conference on Decision and Control, and the European Control Conference*, pages 7931–7936.

Van der Woude, C. and Narasimhan, S. (2010). Dynamic structural modelling of wind turbines using comsol multiphysics.

Wang, X., Foliente, G., Su, Z., and Ye, L. (2006). Multilevel decision fusion in a distributed active sensor network for structural damage detection. *Structural Health Monitoring*, 5(1):45–58.

White, J., Adams, D., and Rumsey, M. (2010). Modal analysis of cx-100 rotor blade and micon 65/13 wind turbine. *Structural dynamics and renewable energy*, 1:15–27.